

Promyelocytic leukemia nuclear bodies behave as DNA damage sensors whose response to DNA double-strand breaks is regulated by NBS1 and the kinases ATM, Chk2, and ATR

Graham Dellaire,^{1,2} Reagan W. Ching,¹ Kashif Ahmed,¹ Farid Jalali,³ Kenneth C.K. Tse,³ Robert G. Bristow,^{3,4,5} and David P. Bazett-Jones¹

¹The Hospital for Sick Children, Toronto, Ontario M5G 1X8, Canada

²Department of Pathology, Dalhousie University, Halifax, Nova Scotia B3H 4R2, Canada

³Ontario Cancer Institute/Princess Margaret Hospital, University Health Network, ⁴Department of Radiation Oncology, and ⁵Department of Medical Biophysics, University of Toronto, Toronto, Ontario M5S 3G4, Canada

The promyelocytic leukemia (PML) nuclear body (NB) is a dynamic subnuclear compartment that is implicated in tumor suppression, as well as in the transcription, replication, and repair of DNA. PML NB number can change during the cell cycle, increasing in S phase and in response to cellular stress, including DNA damage. Although topological changes in chromatin after DNA damage may affect the integrity of PML NBs, the molecular or structural basis for an increase in PML NB number has not been elucidated. We demonstrate

that after DNA double-strand break induction, the increase in PML NB number is based on a biophysical process, as well as ongoing cell cycle progression and DNA repair. PML NBs increase in number by a supramolecular fission mechanism similar to that observed in S-phase cells, and which is delayed or inhibited by the loss of function of NBS1, ATM, Chk2, and ATR kinase. Therefore, an increase in PML NB number is an intrinsic element of the cellular response to DNA damage.

Introduction

The promyelocytic leukemia (PML) protein and PML nuclear bodies (NBs) are implicated in several cellular processes, including transcriptional regulation, tumor suppression, apoptosis, DNA repair, and the replication of both viral and cellular DNA (for reviews see Zhong et al., 2000; Everett, 2001; Salomoni and Pandolfi, 2002; Dellaire and Bazett-Jones, 2004). How they contribute to these nuclear activities, however, has remained elusive. In normal mammalian cells, the PML protein coaccumulates in 5–30 NBs (Dellaire and Bazett-Jones, 2004)

with as many as 75 other proteins (listed in the Nuclear Protein Database; Dellaire et al., 2003). Rather than just sequestering these proteins, there is compelling evidence that the bodies serve as sites for the posttranslational modification of nuclear proteins. For example, the coaccumulation of p53, CBP, and HIPK2 in PML NBs contributes to the regulated phosphorylation (by HIPK2) and acetylation (by CBP) of p53 in response to DNA damage (D'Orazi et al., 2002; Hofmann et al., 2002).

The structural and dynamic behavior of PML NBs is intimately linked to the cell's chromatin integrity (Eskiw et al., 2004; Dellaire et al., 2006). Extensive chromatin contacts on the periphery of the protein cores of the NBs may account for their positional stability through extended periods in interphase of the cell cycle. Physical contacts with chromatin may be important for their proposed role in DNA replication. For example, early transcription and replication of the genomes of several DNA viruses occur immediately adjacent to PML NBs (Everett, 2001). A link between PML NBs and chromatin is also demonstrated in the maintenance of telomeres through a recombination mechanism called alternative lengthening of telomeres,

Correspondence to David P. Bazett-Jones: dbjones@sickkids.ca

Abbreviations used in this paper: ANOVA, analysis of variance; AT, ataxia telangiectasia; ATLD, AT-like disorder; ATM, ataxia telangiectasia mutated; ATR, AT and Rad3-related; DSB, double-strand break; ESI, electron spectroscopic imaging; Gy, Gray; GFP, green fluorescent protein; ICD, interchromatin domain; IF, immunofluorescence; IR, ionizing radiation; LM, light microscopy; LSM, laser scanning confocal microscopy; MEF, murine embryonic fibroblast; MRN, Mre11–Rad50–Nbs1; NB, nuclear body; NBS, Nijmegen breakage syndrome; NHDF, normal human diploid fibroblasts; PK, protein kinase; PML, promyelocytic leukemia; ROI, region of interest; RPA, replication protein A; SUMO, small ubiquitin-like modifier.

The online version of this article contains supplemental material.

whereby a subset of PML NBs in late S/G2 phase become associated with nascent DNA synthesis, DNA repair factors, and telomere proteins (Yeager et al., 1999; Grobelny et al., 2000). The connection between PML NBs and chromatin also extends to a possible role for PML NBs in DNA repair mechanisms. For example, after DNA damage, several DNA repair factors transit to and from PML NBs, and the bodies themselves have been reported to colocalize with sites of unscheduled DNA synthesis in damaged cells (Dellaire and Bazett-Jones, 2004). PML may also function in DNA damage signaling because PML-null cells fail to fully activate p53 in response to DNA damage (Guo et al., 2000) and the PML protein is phosphorylated in response to DNA double-strand breaks (DSBs) by Chk2 (Yang et al., 2002) and ataxia telangiectasia and Rad3-related (ATR) kinase (Bernardi et al., 2004). It is unclear whether these modifications of PML or PML NB composition are critical for DNA repair to proceed or are a consequence of ongoing repair. Regardless, PML NBs are clearly more than passive accumulations of nuclear proteins.

We propose in this study that PML NBs can be used to monitor the topological state and integrity of chromatin in mammalian cells. In so doing, they act as sensors of DNA damage. Previously, we have shown that when the topological state of chromatin is altered during early S phase by the replication of DNA, PML NBs lose both radial symmetry and integrity, fragmenting into “microbodies” by a fission mechanism (Dellaire et al., 2006). We demonstrate a similar response of PML NBs after the introduction of DNA DSBs, thereby providing a basis for previous observations of increases in PML NB number after DNA damage with ionizing radiation (IR; Carbone et al., 2002; Xu et al., 2003). We demonstrate that PML NB breakdown occurs in two components. The first is a rapid biophysical response, occurring in cells damaged at 4°C, a state in which ongoing DNA repair is inhibited, and a second component associated with repair mechanisms. Inactivation or loss of repair factors, such as Nbs1 or the checkpoint kinases ataxia telangiectasia mutated (ATM), Chk2, and ATR, inhibits PML microbody formation in response to DSBs. We suggest that the PML NBs are highly sensitive DNA damage sensors whose dynamic behavior reflects both the degree of DNA damage and the integrity of the DNA repair pathways involved in maintaining the mammalian genome.

Results

The increase in PML NB number in response to DSBs is sensitive, rapid, and dose dependent

The mechanism responsible for an increase in PML NBs after DNA damage (Carbone et al., 2002; Xu et al., 2003) has not been elucidated. To address specifically how DSBs might contribute to this process, we characterized the response of PML NBs to DSBs in the normal human diploid fibroblast (NHDF) cell line GM05757 using IR, etoposide (VP16), and doxorubicin (Fig. 1). IR generates both single-strand breaks and DSBs in DNA, whereas the topoisomerase II inhibitors VP16 and doxorubicin primarily create DSBs (for review see Kurz and Lees-

Miller, 2004). PML NBs were counted in maximum-intensity Z projections of individual cells. In agreement with previous work, we found that PML NB number increased after DSB induction (Fig. 1 A). Furthermore, we found that the time point associated with the highest number of PML NBs coincided with the peak of H2AX phosphorylation (γ -H2AX; Fig. 1 B), an event that occurs on chromatin surrounding DSBs (Rogakou et al., 1999). Maximum PML NB number correlated with peak γ -H2AX signal regardless of the method of DSB induction, suggesting that the increase in PML NB number is coupled to DSB formation. PML NB induction was most rapid for IR, peaking at 30 min after IR (Fig. 1, C and D). In contrast, γ -H2AX signal and PML NB number peaked later, 3 h after treatment with VP16 or doxorubicin (Fig. 1, B–D). Consistent with previous studies of PML NB association with γ -H2AX and components of the Mre11–Rad50–Nbs1 (MRN) complex (Carbone et al., 2002; Xu et al., 2003), we observed foci of γ -H2AX and Nbs1 that partially colocalized with or were juxtaposed to PML NBs between 6 and 18 h after DSB induction (Fig. 1 B and Fig. S1 A, available at <http://www.jcb.org/cgi/content/full/jcb.200604009/DC1>). In contrast, we observed a much earlier colocalization and juxtaposition between the foci of RPA and PML NBs at 1.5 h after DSB induction, which persisted for up to 18 h (Fig. S1 B). After etoposide treatment, only a subpopulation of cells in S and G2 phase develop replication protein A (RPA) foci in NHDFs. Therefore, the association of PML NBs with RPA foci after DNA damage is restricted to S and G2 phase of the cell cycle (Fig. S1 C).

We then tested whether the increase in PML NB number in response to DSBs is dose dependent by treating cells with doses of IR varying from 0–10 grays (Gy; Fig. 1, E and F). We found that at doses as low as 1 Gy (i.e., producing \sim 35 DSBs; Bristow and Hill, 2005), PML NBs increased in number in NHDFs, and the response was dose dependent, based on analysis of variance (ANOVA) between our datasets (Table S1, available at <http://www.jcb.org/cgi/content/full/jcb.200604009/DC1>). In contrast to low doses of IR, where the number of PML NBs returned to baseline levels by 24 h after irradiation, at higher doses of 5 and 10 Gy, PML NB numbers remained elevated for an extended period of time (Fig. 1, E and F). Therefore, after low doses of IR, the increase in PML NB number after DNA damage appears to be reversible. When PML NB number is plotted versus dose of IR, NB number appeared to reach a plateau at doses of 5 Gy or above for all time points, with the exception of 24 h (Fig. 1 F). Therefore, PML NB number varies with the power of the dose of IR and can be described by the modified power function, $y = a \times b^x + c$, where y is the number of PML NBs and x is the dose of IR in grays (Fig. S2 A). Thus, the increase in PML NB number in response to DSBs is rapid, sensitive to sublethal levels of DNA damage, and dose dependent.

PML protein and NB dynamics in response to DSBs

The dynamics of PML NBs after DSB induction with VP16 was examined by live cell analysis of U-2 OS cells stably expressing PML isoform IV (Fig. 2). We found that within 5 min after addition of VP16, new and smaller PML-containing structures

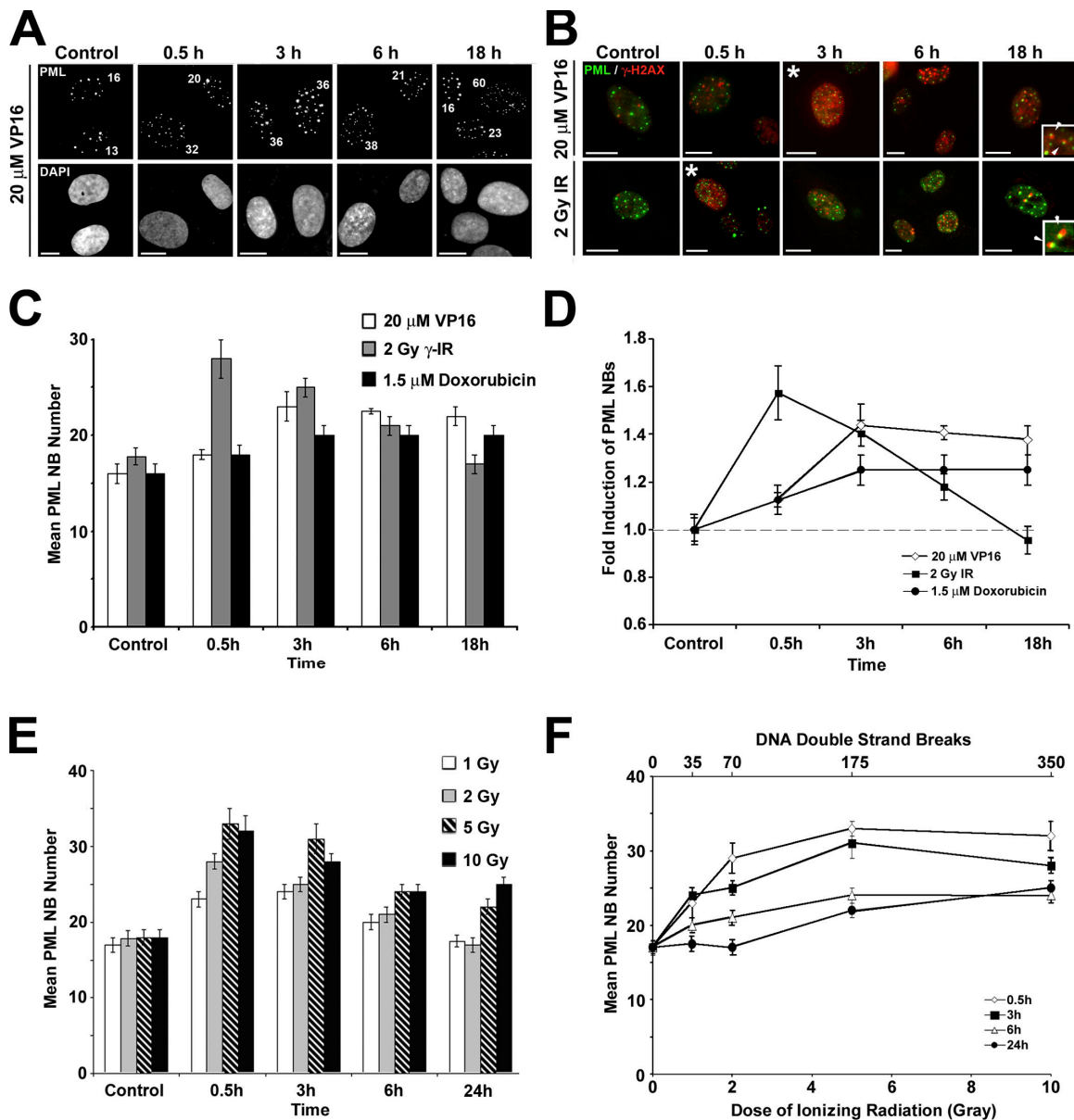


Figure 1. **PML NB number increases in response to DSBs in NHDFs.** NHDF cells (GM05757) were treated with varying doses of IR, etoposide (20 μ M VP16), or 1.5 μ M doxorubicin for 30 min to induce DSBs. (A) IF analysis of PML NB number in maximum-intensity Z projections of NHDFs after etoposide; time after treatment is indicated in hours. (B) IF analysis of the distribution of PML NBs in relation to DSBs in NHDFs after 2 Gy IR or VP16. γ -H2AX is used as a marker for chromatin containing DSBs, and asterisks mark the time points in which the maximum fluorescence intensity of γ -H2AX was first detected. Arrowheads indicate juxtaposition of γ -H2AX and PML NBs at 18 h after DNA damage (inset). Images represent a single focal plane. (C) Comparison of mean PML NB number over time after IR, VP16, and doxorubicin treatment. (D) Comparison of fold increase in PML NB number over time after IR, VP16, and doxorubicin treatment. (E and F) Response of PML NBs to graded doses of IR expressed as a function of time (E) or at each time point as a function of dose (F). Bars, 5 μ m.

began to appear adjacent to the larger PML NBs that were present before treatment (Fig. 2 A). These new bodies, which we term microbodies, arise from preexisting PML NBs by a supra-molecular fission mechanism, as confirmed by spinning-disc confocal microscopy (Fig. 2 B and Video 1, available at <http://www.jcb.org/cgi/content/full/jcb.200604009/DC1>). This fission mechanism is similar to that observed for new PML NB formation in early S phase (Dellaire et al., 2006), as PML NB's biochemical composition was initially indistinguishable between microbodies and the larger parental PML NBs, in respect to Sp100 and small ubiquitin-like modifier (SUMO-1) content (Fig. S3).

However, although Sp100 levels at PML NBs did not change over the time course observed (Fig. S3 A), we did notice a reproducible drop in SUMO-1 levels in PML NBs at 3 h after VP16 treatment (Fig. S3, B and C). Overexpression of SUMO-1 dramatically reduced PML NB number (Fig. S3 D), resulting in enlarged bodies that showed reduced or delayed increase in PML NB number in response to DSBs (Fig. S3 E). It is unclear if overexpression of SUMO-1 is directly or indirectly responsible for the stabilization of PML NBs in our experiments because sumoylation is implicated in many biological pathways, including DNA repair (Gill, 2004).

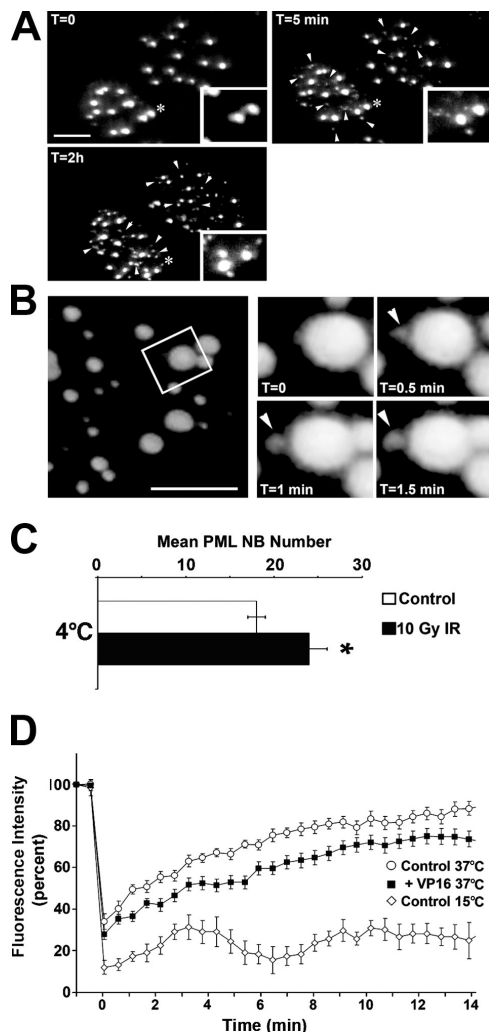


Figure 2. PML protein and PML NB dynamics after DSB induction. (A) PML microbody formation occurs rapidly after treatment with etoposide. Two U-2 OS human osteosarcoma cells stably expressing GFP-PML IV protein were imaged by fluorescence microscopy before ($T = 0$) and after addition of etoposide ($20 \mu\text{M}$ VP16; $T = 5$ min and $T = 2$ h). Enlarged region of the cell marked by white asterisk is shown at each time point. White arrowheads indicate newly formed microbodies after VP16 treatment. (B) Formation of PML microbodies in response to DNA DSBs occurs by supramolecular fission from preexisting parental PML NBs. A U-2 OS cell expressing GFP-PML IV was visualized before ($T = 0$) and during treatment with $20 \mu\text{M}$ VP16 over several minutes ($T = 0.5$, 1.0, and 1.5 min are shown). Arrowhead indicates fission of a PML microbody from a larger parental PML NB. (C) PML NBs increase in number in cells irradiated on ice. NHDFs (GM05757s) were incubated on ice for 20 min and either fixed (Control) or irradiated on ice (10 Gy IR) before fixation. Mean PML NB number increases significantly between control (17 ± 1 ; $n = 30$) and cells irradiated with 10 Gy IR on ice (24 ± 2 ; $n = 30$; *, $P = 0.0008$). (D) Dynamics of the PML protein within PML NBs is affected by DNA damage and reduced temperature. Asynchronous U-2 OS GFP-PML IV cells were subjected to treatment with etoposide ($20 \mu\text{M}$ VP16 for 30 min) before mobility of PML protein within PML NBs was analyzed by FRAP at 37°C ($n = 20$). Mobility of the PML protein at PML NBs in DNA damaged cells is compared with control untreated cells ($n = 20$) at 37°C and at 15°C ($n = 7$). Data are presented as the mean fluorescence recovery plotted as percent of initial fluorescence intensity of the PML NB over 14 min. Error bars represent the standard error. Bars, $5 \mu\text{m}$.

PML microbodies also formed immediately after irradiation with doses as low as 1 Gy of IR (unpublished data), and an increase in PML NB number was seen even when cells were

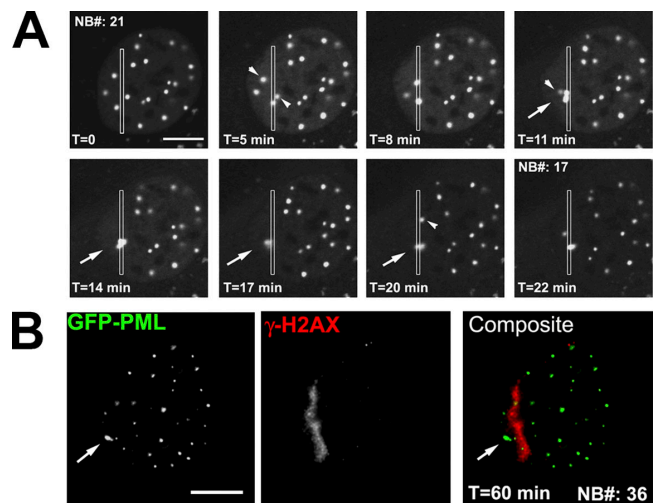


Figure 3. PML NBs lose positional stability when chromatin is damaged in their vicinity. (A) UV laser-induced DSBs alter the positional stability of PML NBs. A single U-2 OS cell expressing GFP-PML IV is shown, in which DSBs were created in a laser track along a defined ROI ($\sim 0.5 \times 10 \mu\text{m}$; rectangular box) by photoinduction; PML NB movement was tracked over time. PML NBs (arrowheads) along the laser path (rectangular box) move toward and aggregate with one large PML NB (arrow) adjacent to the laser track. PML NB number (NB#) is shown before laser induction of DSBs and 22 min after induction. (B) Confirmation of laser-induced DSBs by IF detection of $\gamma\text{-H2AX}$. The same cell shown in A was fixed at 60 min after laser induction of DSBs and processed for immunodetection of PML and $\gamma\text{-H2AX}$. PML NB number at this time point is indicated (NB#). Bars, $5 \mu\text{m}$.

irradiated and fixed on ice to prevent diffusional movement of PML protein or ongoing DNA repair (Fig. 2 C). At temperatures $<15^\circ\text{C}$, PML protein diffusion is very limited, as confirmed by FRAP analysis (Fig. 2 D). Interestingly, we also observed a 10% difference in the maximum fluorescence recovery between control and etoposide-treated cells, consistent with a larger immobile fraction of PML protein in bodies after DNA damage (Fig. 2 D).

We next examined the behavior of PML NBs in the vicinity of site-specific DSBs induced by UV laser irradiation (Fig. 3, A and B; and Video 2, available at <http://www.jcb.org/cgi/content/full/jcb.200604009/DC1>). Within 5 min of the induction of DSBs, PML NBs in the vicinity of the laser track began to move and coalesce (Fig. 3 A, arrowheads). This process continued for over 20 min, resulting in a drop in PML NB number from 21 to 17 NBs, but did not affect PML NBs distal to the laser track (Fig. 3 A). At later time points, however, even PML NBs far from the laser track lost their positional stability. Imaging of cells in the absence of UV laser microbeam irradiation did not affect the mobility or number of PML NBs (Video 3). Continuous imaging by laser scanning confocal microscopy (LSM) after DNA damage did not reveal microbody formation, likely because of photobleaching and the loss of visibility of small, PML-containing structures. However, after fixation and immunofluorescence (IF) detection of PML and $\gamma\text{-H2AX}$ by wide-field microscopy 1 h after photoinduction of DNA DSBs, it was apparent that the DNA damage was confined to the laser track and that PML NB number had increased from 17 to 36 PML NBs (Fig. 3 B). Although wide-field microscopy is generally

more sensitive than LSM in the detection of PML microbodies, we found that LSM was sufficient to detect >90% of bodies within a focal plane (unpublished data). Therefore, the increase in the number of PML NBs at 1 h after DSB induction is primarily caused by microbody formation.

Structural destabilization of PML NBs correlates closely with topological changes in chromatin after DNA damage

To address the ultrastructural changes in PML NBs after DNA damage, we used immunogold detection of PML with correlative light microscopy (LM) and electron spectroscopic imaging (ESI; Dellaire et al., 2004; Fig. 4). Using LM/ESI we observed that, in control NHDFs, PML NBs exhibit radial symmetry and make extensive contacts with the surrounding chromatin (Fig. 4A). Upon treatment with VP16, we found that PML NBs lose their radial symmetry and make fewer contacts with the surrounding chromatin fibers. We also observed “microbody-like” structures, which were identified by immunogold detection of PML, adjacent to chromatin in the vicinity of larger “parental” PML NBs (Fig. 4, B and C). A much larger interchromatin domain space was also apparent in cells treated with VP16 (black spaces outside of chromatin in Fig. 4). These changes in both chromatin and PML NBs are reminiscent of those seen in cells entering S phase (Dellaire et al., 2006). Based on these results, we suggest that the introduction of DSBs results in topological changes in chromatin linked to PML NBs, which destabilizes the PML NB core.

The increase in PML NB number in response to DSBs does not require p53 or ongoing protein translation

PML protein levels can increase after treatment with IR in a p53-dependent manner (de Stanchina et al., 2004). Therefore, we examined the PML NB response to DNA DSBs in NHDFs with inhibition of PML protein synthesis by treatment with cycloheximide, and in cells that lack a functional p53 pathway (i.e., null p53 human Saos-2 osteosarcoma cells and paired HCT116 cell lines, which were isogenic save for p53 protein; Fig. 5). We found that PML protein levels increased slightly, by 1.3-fold at 4 h after VP16 treatment, and that they reached 1.8-fold by 12 h (Fig. 5 A). As expected, cycloheximide treatment inhibited the DNA damage-dependent increase in PML protein levels at 12 h, but had little effect at 4 h, suggesting that post-translational regulation of PML protein levels may occur at this earlier time point. We found that inhibition of protein synthesis or loss of p53 function did not prevent the initial increase in PML NB number (at 30 min and 3 h) in response to DSBs (Fig. 5, B–C). Loss of p53 in the HCT116 cell background actually appeared to enhance the increase in PML NB numbers at 30 min after VP16 treatment (Fig. 5 C), perhaps because further genome instability from a concurrent loss of the mismatch repair factor MLH1 (Koi et al., 1994).

Cycloheximide-treated NHDFs exhibited a higher number of PML NBs initially, compared with untreated cells, and NB number returned to control levels much earlier than in untreated NHDFs (Fig. 5 B). In contrast, PML NB number in

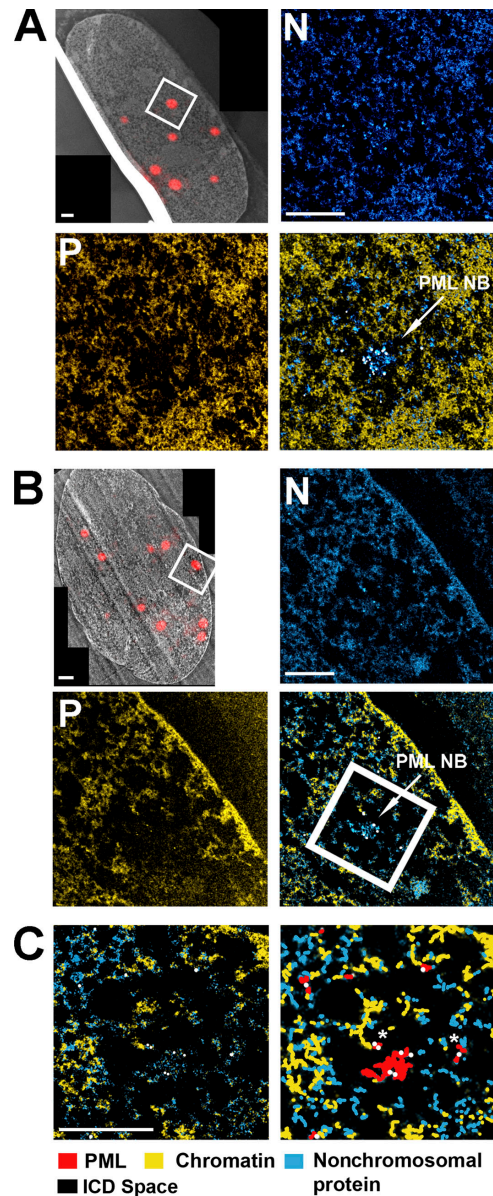


Figure 4. Ultrastructural analysis of PML NBs in NHDFs by correlative LM/ESI before and after etoposide-induced DNA damage. Regions of interest containing a PML NB, which are shown at higher magnification in subsequent images, are delineated by white boxes. (A) LM/ESI of a single NHDF (GM05757) cell, fluorescently labeled for PML protein. Elemental maps of nitrogen (N) and phosphorus (P), and the merged maps of a PML NB and its surrounding nucleoplasm reveal protein-based (cyan) and nucleic acid-based (yellow) components. Chromatin appears yellow in the merged image because of high N and P content. A single PML NB is shown at higher magnification (cyan, as indicated by the arrow) making many contacts to the surrounding chromatin (yellow), and has radial symmetry typical of PML NBs in unstressed cells. (B) LM/ESI of a single NHDF (GM05757) treated with 20 μ M etoposide (VP16) for 30 min, fluorescently labeled for PML protein. After treatment with VP16, the protein core of PML NB is disrupted in response to DSB induction; few contacts with chromatin remain, and radial symmetry is lost. (C) PML NB in B, at higher magnification (left), and a cartoon representation of the same EM micrograph (right), where PML protein-containing protein structures (red), chromatin (yellow), and other nonchromosomal protein (blue) are shown. Redistribution of PML microbodies along chromatin fibers (asterisks) is observed, and larger interchromatin spaces (black areas) are apparent. PML protein localization was determined by immunogold detection of PML (white dots). Bars, 500 nm.

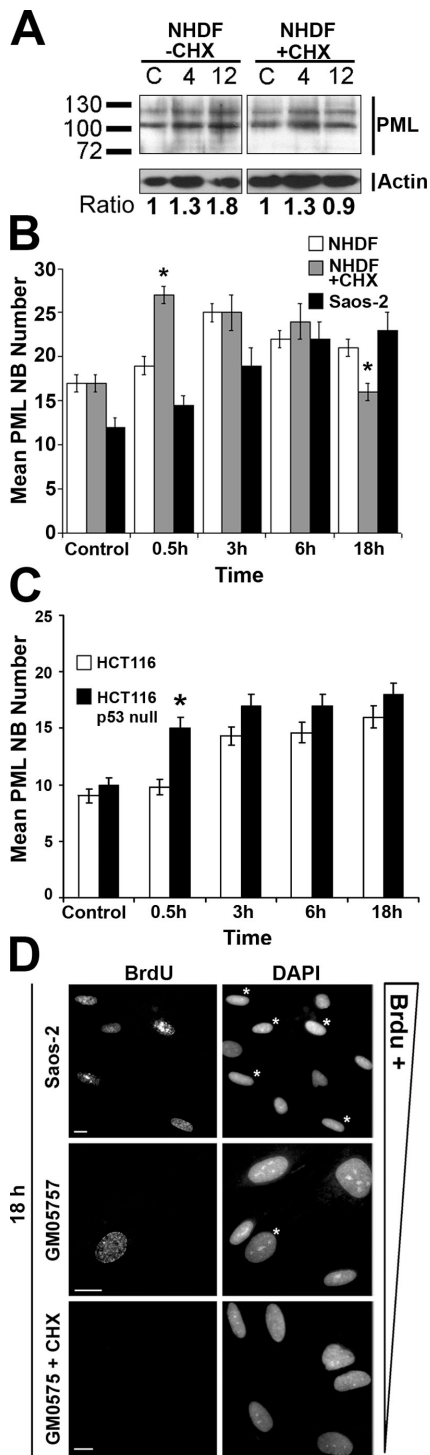


Figure 5. The increase in PML NB number in response to DSBs is independent of new protein translation and p53. NHDF cells (GM05757) in the presence or absence of 150 μ M cycloheximide (CHX), Saos-2 human osteosarcoma cells, and isogenic HCT116 human colon carcinoma cells (+ or - p53) were treated with etoposide (20 μ M VP16) for 30 min (*, $P < 0.0001$). (A) Western blot analysis of PML protein levels after etoposide treatment in the presence or absence of cycloheximide. NHDFs were treated with etoposide (20 μ M VP16 for 30 min) and harvested at the indicated times for SDS-PAGE and Western blot analysis. Ratio of PML protein levels in the control lane to PML protein at the indicated time points after etoposide treatment are shown normalized against actin. (B) Comparison of mean PML NB number after VP16 treatment in NHDFs, NHDFs treated with cycloheximide (+CHX), and Saos-2 cells. (C) Comparison of mean PML NB number after VP16 treatment in isogenic HCT116 and HCT116

VP16-treated Saos-2 cells continued to increase over time (Fig. 5 B). PML NB number is affected by cell cycle progression and increases in early S phase (Dellaire et al., 2006). FACS analysis revealed that after VP16 treatment, NHDFs showed a marked accumulation in G1 and G2 phase of the cell cycle by 18 h (Fig. S4 A, available at <http://www.jcb.org/cgi/content/full/jcb.200604009/DC1>). Therefore, differences in the number of cells in S phase at the late time points (6 and 18 h) might account for the continued increase in PML NBs observed in the G1/S checkpoint-deficient Saos-2 cells. We examined this possibility by detecting BrdU incorporation at 18 h after VP16 treatment to determine the fraction of cells replicating DNA (Fig. 5 D). We estimate that ~40% of the Saos-2 cells were in S phase, compared with only 5–6% of NHDFs, and no BrdU incorporation was observed in NHDFs treated with cycloheximide. Therefore, at early time points, the increase in PML NB number is independent of both new protein synthesis and p53. However, at later time points after DNA damage, PML NB number is sensitive to loss of p53 caused by abrogation of the G1/S checkpoint, and as a result, PML NB number continues to increase as cells enter S phase inappropriately.

The increase in PML NB number in response to DSBs is abrogated by caffeine and inhibited by the loss of function of Nbs1, ATM, Chk2, and ATR kinase

Because ATM, ATR, and Chk2 kinase are key regulators of the cellular response to DNA damage (Shiloh, 2001; Pommier et al., 2005), we examined whether chemical inhibition of these kinases might affect the response of PML NB to DSBs in NHDFs (Fig. 6 A). Inhibition of ATR and ATM kinase by 5 mM caffeine had an inhibitory effect on the increase of PML NB number after VP16 treatment at all time points ($P < 0.0001$; Fig. 6 A). Similarly, caffeine significantly reduced the response of PML NBs to 5 Gy of IR ($P < 0.001$; Fig. S4 B). This effect was not caused by caffeine-dependent changes in the cell cycle profile because PML NB number did not change when cells were pretreated with caffeine for 30 min before induction of DSBs (Fig. 6 A), and only prolonged treatment with caffeine had an effect on the cell cycle profile of NHDFs, with or without VP16 treatment (Fig. S4, A and C, 18 h). Pretreatment of NHDFs with the Chk2 kinase inhibitor II (Arienti et al., 2005) did not affect the initial increase in PML NBs in response to VP16, but did significantly reduce the number at 3 h, compared with cells treated with VP16 in the absence of inhibitor ($P < 0.0003$; Fig. 6 A). Similarly, 20 μ M wortmannin, which strongly inhibits DNA-PK and ATM kinase, but weakly inhibits ATR, had a significant effect on PML NB number only at 3 h after VP16 treatment ($P < 0.001$; Fig. 6 A). In contrast, the DNA-PK inhibitor LY2942002 had little effect on PML NB number in response to DSBs.

p53-null cells. (D) Comparison of DNA synthesis activity of NHDFs, NHDFs treated with cycloheximide (+CHX), and Saos-2 cells at 18 h after VP16 treatment. 18 h after VP16 treatment, cells were incubated with BrdU, fixed, and processed for immunodetection of BrdU, and DNA was counterstained with DAPI. Asterisks represent BrdU-positive cells. Bars, 5 μ m.

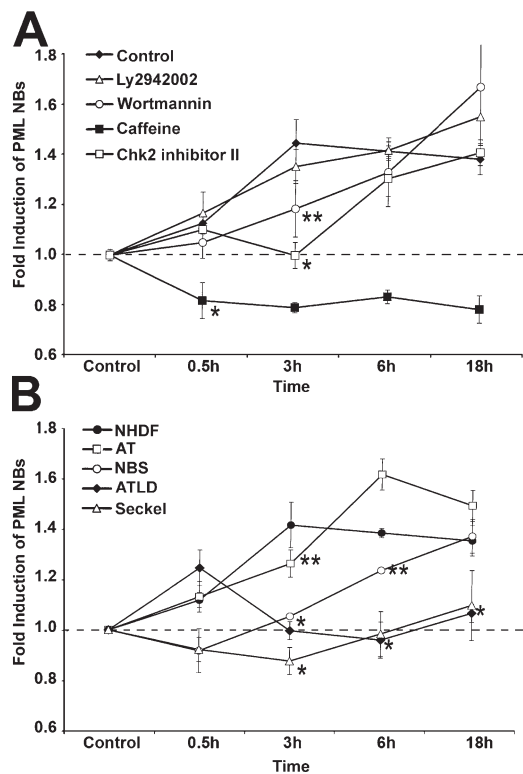


Figure 6. The increase in PML NB number in response to DSBs is delayed or inhibited in the presence of PI3 kinase inhibitors and in DNA repair-deficient cell lines. (A) Comparison of effects of DNA repair kinase inhibitors on the increase in PML NB number in response to DSBs. NHDF cell line GM05757 (control) was pretreated with 10 μ M Chk2 kinase inhibitor (Chk2 inhibitor II) or various PI3 kinase inhibitors (5 mM caffeine, 20 μ M wortmannin, or 50 μ M LY2942002) for 30 min before treatment with etoposide (20 μ M VP16 for 30 min; *, $P < 0.0001$; **, $P < 0.001$). (B) Comparison of the fold increase in PML NB number after etoposide treatment (20 μ M VP16 for 30 min) in NHDF cells and DNA repair-deficient human fibroblast cell lines. AT, ataxia telangiectasia; NBS, Nijmegen breakage syndrome; ATLD, AT-like disorder; Seckel, Seckel syndrome. *, $P < 0.0001$; **, $P < 0.02$.

We also treated several repair-deficient cell lines with VP16 to compare the PML NB response after DNA damage. As with chemical inhibition of ATM, AT cells, which are deficient in ATM, showed a significant inhibition of PML NB number increase only at 3 h after VP16 treatment ($P < 0.02$; Fig. 6 B), after which PML NB number actually increased beyond that expected for NHDFs at 6 h. AT-like disorder (ATLD) cells expressing mutant Mre11 (Stewart et al., 1999), which is a component of the DNA damage sensor known as the MRN complex (D'Amours and Jackson, 2002), showed an initial increase in PML NB number after VP16 treatment at 30 min, which is similar to NHDFs. At the 3-h time point and thereafter, however, the increase in PML NB number was inhibited by loss of Mre11 function ($P < 0.0001$; Fig. 6 B). The increase in PML NB number after induction of DSBs was significantly inhibited at all time points observed in Nijmegen breakage syndrome (NBS) cells, which are deficient in Nbs1, which is also a member of the MRN complex (Carney et al., 1998), and was profoundly inhibited in Seckel syndrome cells, which are deficient in ATR kinase ($P < 0.0001$; Fig. 6 B; O'Driscoll et al., 2003).

Because the concentration of Chk2 inhibitor used in our experiments could have residual effects on other kinases (<25% inhibition of a panel of 35 kinases, Arienti et al., 2005), we wished to confirm the role of Chk2 in regulating the response of PML NBs to DSBs using a genetic mouse model. As predicted from our inhibitor data, Chk2 $-/-$ murine embryonic fibroblasts (MEFs) had an abrogated PML NB response to DSBs, compared with isogenic wild-type MEFs at 3 h after VP16 treatment ($P < 0.001$; Fig. 7 A). Similarly, reconstitution of NBS cells with wild-type human Nbs1 by retroviral transduction resulted in a robust increase in NB number at 3 h after VP16 treatment, confirming a role for Nbs1 in regulating the PML NB response to DSBs ($P < 0.02$; Fig. 7 B). Finally, we further characterized the role of ATR kinase in regulating the response of PML NBs to DSBs by VP16 treatment of U-2 OS cells expressing an inducible dominant-negative mutant of ATR (kinase-dead ATR-DN; Fig. 7 C; Nghiem et al., 2001). Induction of ATR-DN in these U-2 OS cells for 24 h before VP16 treatment significantly inhibited PML NB induction at 30 min, 3 h ($P < 0.0001$), and 6 h after treatment ($P < 0.001$; Fig. 7 C). Interestingly, PML NB numbers continued to rise in U-2 OS cells expressing the ATR-DN protein, possibly because of extensive genome instability and eventual apoptosis associated with prolonged expression of this protein. Even within the population of U-2 OS cells expressing the ATR-DN protein, high expression correlated with reduced PML NB number, compared with low-expressing cells at 3 h after VP16 treatment (Fig. 7 C).

Discussion

PML NBs make extensive contacts to chromatin in their vicinity, which accounts both for their positional stability during interphase (Eskiw et al., 2004) and their highly dynamic behavior in S phase, when chromatin topology is altered during DNA replication (Dellaire et al., 2006). Because of their intimate relationship with chromatin, we previously hypothesized that PML NBs might also represent sensors of DNA damage (Dellaire and Bazett-Jones, 2004). In this study, we have systematically tested this hypothesis, demonstrating that PML NBs behave as dose-dependent sensors of DSBs.

PML NBs initially respond to DSBs by increasing in number by fission

Chromatin is physically constrained by subnuclear compartments such as the nucleolus and the nuclear lamina (Chubb et al., 2002). Chromatin contacts on the surfaces of the protein-based cores of PML NBs may also serve as chromatin-anchoring sites (Fig. 8 A). The positional stability of PML NBs and the low rates of chromatin mobility indicate a balance of forces between chromatin and such anchoring sites. Recently, we have shown that chromatin appears to “relax,” or decondense, in the vicinity of DSBs (Kruhlik et al., 2006). This balance of forces, or tensegrity, may be altered by the introduction of DSBs in chromatin, and could lead to the shearing of the PML NB core as the associated chromatin domains pull away from the body. One outcome of this biophysical response is the supramolecular fission of PML NBs into microbodies immediately after the

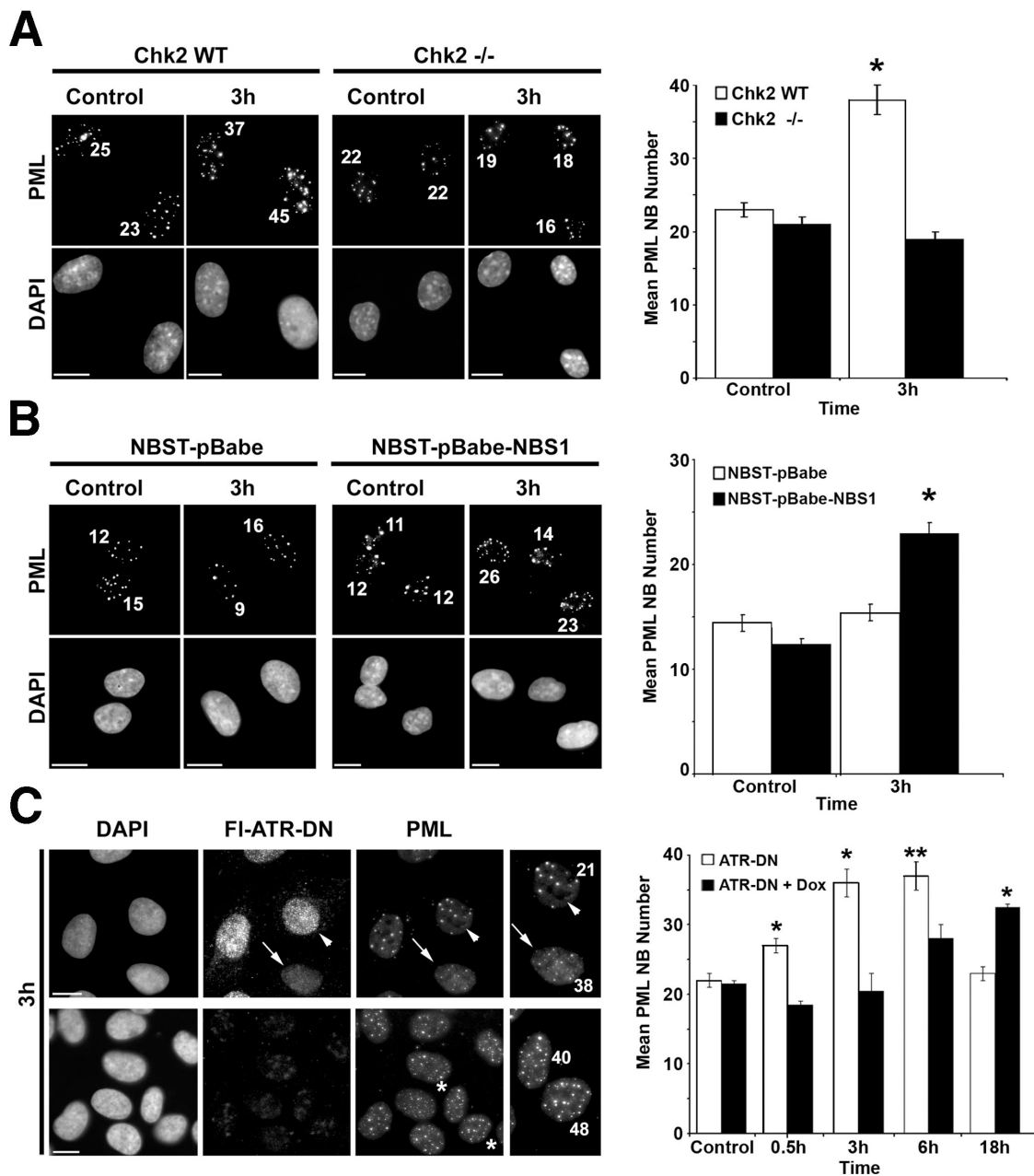


Figure 7. PML NB induction in response to DSBs requires NBS1, Chk2, and ATR-function. Cells were treated with etoposide (20 μ M VP16 for 30 min), left to recover for 3 h, and processed for IF detection of PML. DNA was counterstained with DAPI. PML NB number is indicated in maximum-intensity Z projections of IF images of control and etoposide-treated cells (left) and a comparison of mean PML NB number (right) is shown. Error bars represent the SEM. Bars, 5 μ m. (A) Comparison of the PML NB number between etoposide-treated Chk2-null (Chk2 $-/-$) and wild-type Chk2 (Chk2 WT) MEFs (*, $P < 0.001$). (B) Comparison of PML NB number between Tert-immortalized human NBS fibroblasts infected with an empty retroviral vector (NBST pBabe) or a retroviral vector carrying wild-type human NBS1 (*, $P < 0.02$). (C) Disruption of ATR kinase function inhibits the increase in PML NB number in response to DSBs. U-2 OS cells expressing a doxycycline-inducible, kinase-inactive, dominant-negative ATR kinase (ATR-DN) were treated with (+ Dox) or without doxycycline for 24 h before etoposide treatment. Besides PML, IF detection of ATR-DN (FI-ATR-DN) is also shown. Cells with high ATR-DN expression (arrow) contain fewer PML NBs after etoposide treatment than cells with low expression (arrowhead). White asterisks indicate two cells with similar PML NB number in cells not expressing ATR-DN. DNA was counterstained with DAPI. *, $P < 0.0001$; **, $P < 0.001$.

introduction of DSBs (Fig. 8 B). We propose that the biophysical response to changes in chromatin tensegrity is the primary basis for the fission of PML NBs when cells are irradiated at 4°C (Fig. 2 C), a condition under which biochemical activities, such as DNA repair and biochemical changes to chromatin and PML NBs, are almost entirely blocked (Fig. 8 B). It is unlikely that de novo formation of PML NBs (Everett and Murray, 2005) by

the redistribution of PML protein accounts for the initial increase in the number of PML NBs because protein diffusion is very limited below 15°C (Fig. 2 D). Furthermore, an ultrastructural examination of PML NBs in situ after DSB induction with VP16 revealed that the protein core of the PML NB is indeed destabilized in conjunction with structural changes in chromatin (Fig. 4 B). A similar instability of PML NB structure is observed

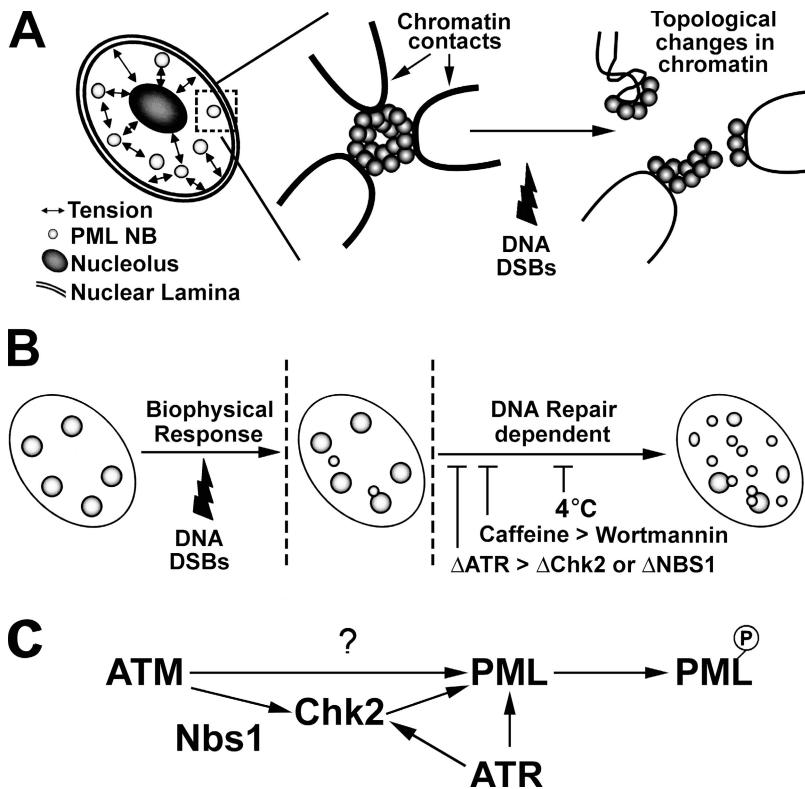


Figure 8. Summary of the biophysical and molecular mechanisms responsible for the increase in PML NB number in response to DSBs. (A) Model of the biophysical effect on PML NBs by changes in chromatin structure or tensegrity. Chromatin is constrained and under tension (double-headed arrows) by tethering to subnuclear compartments such as the nucleolus, nuclear lamina, and, possibly, PML NBs. DSB-induced changes in chromatin structure or tensegrity alter the balance of forces constraining chromatin within the nucleus; this biophysical phenomenon destabilizes PML NBs that are tethered to chromatin, resulting in microbody formation by fission from preexisting NBs. (B) Model for PML NB number increase in response to DSBs. Initially, PML NB number increases because of biophysical changes in chromatin after DSBs, as in A. The second phase of the PML NB response to DNA damage requires ongoing DNA repair processes, which can be inhibited by low temperatures (4°C) by inhibition (caffeine) or loss of function of NBS1 ($\Delta NBS1$) or Chk2 ($\Delta Chk2$), whose activation is affected by inhibition of ATM (wortmannin). (C) Summary of DNA repair kinase pathways implicated in phosphorylation of the PML protein in response to DNA DSBs. It is currently unknown if ATM can directly phosphorylate PML.

in early S phase, where the NBs also break apart by fission (Dellaire et al., 2006).

PML NBs are sensitive detectors of DNA damage

PML NBs behave as DNA damage sensors by increasing in number in response to genotoxic stress. The initial formation of microbodies by a fission mechanism is sensitive to as few as 35 DSBs (1 Gy IR). However, PML NB number does not increase in a linear fashion with the dose of IR, in contrast to the induction of DSBs and, consequently, the phosphorylation of H2AX (Rogakou et al., 1999). At high doses of IR (>5 Gy), PML NB number per cell becomes saturated (Fig. 1 F). We can model the relationship of PML NB number to DSBs as a modified power function, where NB number varies with the power of the dose (Fig. S2 A). This relationship holds for PML NB number up to 6 h after irradiation. In addition, at low doses of IR, PML NB number returns to control levels within 24 h, whereas at high doses of IR (i.e., 5 and 10 Gy), PML NB number remains elevated. Doses of IR at 5 and 10 Gy are considered supra-lethal, as they inhibit cell growth in clonogenic assays by 90–100% (Bristow and Hill, 2005). Therefore, the failure of PML NB number to return to that of control cells after irradiation may be an indication of either eventual senescence or programmed cell death. PML NB number also remains elevated for extended periods after DNA damage in cells that have impaired cell cycle checkpoints (e.g., caused by loss of p53; Fig. 5). Thus, at nonlethal physiological levels of DNA damage, PML NB number may provide a simple indicator of the complex response of mammalian cells to DNA damage and the fidelity of the p53-dependent G1/S checkpoint.

Live cell analysis demonstrates that PML NBs are not recruited to sites of DNA damage

PML NBs appear to associate with single-stranded regions of DNA, as well as with foci containing γ -H2AX and/or repair proteins after DNA damage (Dellaire and Bazett-Jones, 2004). We also observed the juxtaposition of γ -H2AX foci (Fig. 1 B) and the colocalization of Nbs1 with PML NBs at 6 and 18 h after the induction of DSBs (Fig. S2 A). At 1.5 h after DSB induction, we also observed the colocalization and juxtaposition of RPA foci with PML NBs in NHDFs in S and G2 phase of the cell cycle (Fig. S2, B–C). These data raise the possibility that PML NBs and DNA repair proteins may be able to coaccumulate at sites of DNA damage by the movement of intact PML NBs or by their de novo formation. We tested these assumptions by UV laser induction of DSBs in defined regions of the nucleus of U-2 OS cells expressing GFP-PML IV (Fig. 3, A–B). PML NBs in close proximity to the laser-induced DSBs began to lose positional stability and NB number dropped as these “liberated” bodies aggregated with each other. However, we did not see the de novo formation of PML NBs along the length of the laser track, as would be expected if PML were coaccumulating at sites of DNA damage. Thus, although PML NBs lose positional stability when chromatin is damaged in their vicinity, they do not form de novo or move to sites of DNA damage. Rather, they are able to move large distances through the nucleoplasm, possibly through spaces or channels created in chromatin by the extensive number of DSBs created along the laser track (Bradshaw et al., 2005). Such long-range movement of PML NBs is consistent with “corral” models of NB movement within the interchromatin domain space

(Eskiw et al., 2003; Gorisch et al., 2004). Eventually, PML NBs far from the laser track respond by changes in their movement and microbody formation, suggesting that either global changes in chromatin structure are occurring at later time points after DNA damage and/or ongoing DNA repair processes are required for this phenomenon. The colocalization of PML NBs with RPA in G2- and S-phase cells at 1.5 h after DSB induction may indicate a role for PML in homologous recombination events, such as sister-chromatin exchange, in cooperation with other factors, such as BLM (Hu et al., 2001; Rao et al., 2005). The significance of the colocalization and juxtaposition of NBs with γ -H2AX and Nbs1 at late time points after DNA damage (i.e., 6 and 18 h; Fig. S1 A) remains unclear because >90% of DNA repair has already been completed. Perhaps at these late time points, PML NBs may function as sites of posttranslational modification of DNA repair factors at the end of the repair cycle, rather than playing a direct role in the DNA repair mechanisms themselves.

Signaling pathways regulating DNA repair and PML NB response to DSBs share common factors

After the initial rapid formation of PML microbodies by a fission mechanism, further increases in PML NB number accompany ongoing DNA repair. This can be explained by the sensitivity of PML NBs to the topological state of chromatin (Dellaire et al., 2006), which is affected by chromatin remodeling associated with DNA repair (Lydall and Whitehall, 2005). Therefore, mutations in components of the DNA repair response could also abrogate the breakdown of PML NBs into microbodies. ATM and ATR kinases are key regulators of the cellular response to DNA damage, which may play partially redundant roles because they share many of the same substrates, such as Chk2, Brca1, and p53 (for reviews see Shiloh, 2001; Pommier et al., 2005).

We addressed the role of the ATM and ATR DNA repair pathways in regulating the increase in PML NB number in response to DSBs, by using both repair-deficient cell lines and chemical inhibition of ATM, ATR, and Chk2 kinase. AT cells expressing mutant ATM or NHDF treated with wortmannin, which is an inhibitor of ATM, demonstrated a similar delay in the increase in PML NBs in response to DSBs, which was most significant at 3 h after VP16 treatment (Fig. 6 A–B). A similar delay in the increase in PML NB number occurred at 3 h in NHDFs treated with a Chk2-specific kinase inhibitor (Fig. 6 A) and in Chk2 $-/-$ MEFs (Fig. 7 A). We also found that loss of Nbs1, which is a member of the MRN DNA damage-sensing complex (D'Amours and Jackson, 2002) and is required for activation of Chk2 by ATM in response to low levels of DNA damage (Buscemi et al., 2001), caused a significant delay in the increase in PML NB number in response to VP16 (Fig. 6 B and Fig. 7 B). Therefore, the inhibition of PML microbody formation in NBS or AT cells at 3 h after etoposide treatment (Fig. 6 B) may result, in part, from a failure to activate Chk2 in response to DSBs. In addition, chromatin topology changes after DNA damage may be subject to regulation by ATM kinase (unpublished data; Shiloh, Y., personal communication).

Therefore, ATM's role in regulating PML NB behavior after DNA damage could be twofold, (a) through the activation of Chk2 and (b) via modulation of chromatin topology after DNA damage.

NBS cells also initially had many fewer PML NBs at 30 min after VP16 treatment compared with ATM- or Chk2-deficient cells. In contrast, Mre11-deficient ATLD cells showed an initial increase in PML NB number similar to NHDFs, followed by a significant reduction in PML NB number at all other time points. Because Nbs1 and Mre11 are in the same DNA damage-sensing complex, the basis for this discrepancy between NBS and ATLD cells in regard to PML NB induction is unclear. An intriguing possibility is that Nbs1 may play an earlier and separate role in regulating the increase in PML NB number in response to DSBs beyond the activation of Chk2.

PML NB number after VP16 treatment was inhibited to an even greater extent in Seckel syndrome cells deficient in ATR (O'Driscoll et al., 2003) than for cells deficient in ATM, Chk2, or Nbs1 (Fig. 6 B). In addition, the dominant-negative inhibition of ATR kinase by expression of a kinase-dead mutant of ATR (ATR-DN; Fig. 7 C) in U-2 OS cells also inhibited the increase in PML NB number in response to DSBs. The most dramatic inhibition, however, occurred when we inhibited both ATM and ATR with caffeine (Fig. 6 A). At all time points after DSB induction, PML NB number remained at or below that of untreated cells. The additive effect of inhibition of ATM- and ATR-dependent pathways on the increase in PML NB number in response to DSBs by caffeine suggests they act in parallel pathways, which is consistent with their redundant roles in regulating DNA damage checkpoints (Shiloh, 2001). Although the initial biophysical response of PML NBs is dependent on changes in the tensegrity and topological state of chromatin associated with DSB induction and DNA repair, it remains an intriguing possibility that ATR- or Chk2-dependent phosphorylation of PML and PML NB constituents (Yang et al., 2002; Bernardi et al., 2004) may also contribute to NB instability (Fig. 8 C). Other forms of DNA damage, such as UV irradiation (Seker et al., 2003), also appear to destabilize PML NBs. Because ATR kinase is strongly activated by UV irradiation, DNA single-strand breaks, and drugs that induce replication fork stalling (Shiloh, 2001), it is likely that the increase in PML NB number seen in response to these cellular stresses is also regulated by ATR kinase. We are currently testing this hypothesis.

In summary, we have demonstrated that PML NBs are, indeed, dynamic sensors of DNA damage that respond to DNA DSBs by increasing in number, primarily by a fission mechanism. The DSB-dependent increase in PML NBs occurs first as a biophysical response to changes in chromatin. However, soon after DSB induction, PML NB number becomes sensitive to cell cycle checkpoint control and ongoing DNA repair, being regulated by ATR kinase and, to a lesser extent, ATM kinase, possibly through Nbs1-dependent activation of Chk2 kinase. This dynamic behavior of PML NBs in mammalian cells provides an exceptional pathological marker for cellular health, cell cycle progression, and the integrity and stability of the genome.

Materials and methods

Cell culture and drug treatments

Cell lines used in this study are as follows: NHDFs (GM05757; Coriell Cell Repository); human AT fibroblasts (AT5B1 and GM05823; Coriell Cell Repository); human NBST fibroblasts (gift from J. Lukas, Danish Cancer Society, Copenhagen, Denmark); human ATLD fibroblasts (gift from Y. Shiloh, Tel Aviv University, Tel Aviv, Israel); Saos-2 (American Type Culture Collection [ATCC]); HCT116 and p53-null HCT116 isogenic cells (gift from B. Vogelstein, Johns Hopkins University, Baltimore, MD); ATR-DN and ATR-WT cells (gift from Paul Nghiem, University of Washington Medical School, Seattle, WA); Seckel syndrome cells (GM18366; Coriell Cell Repository); Chk2 $-/-$ MEFs and isogenic WT MEFs (gift from T. Mak, University of Toronto, Toronto, Canada); and isogenic and U2OS cells stably expressing GFP-PML IV (gift from J. Taylor, University of Wisconsin, Milwaukee, WI). NBST-pBabe and NBST-pBabe-NBS1 cell lines were generated by retroviral transduction of NBST fibroblasts using either pBabe-Puro alone or encoding full-length human Nbs1 (gift from J. Lukas), respectively. To generate DSBs, cells were treated with 20 μ M etoposide (VP16; Sigma-Aldrich) or 1.5 μ M doxorubicin (Sigma-Aldrich) for 30 min, washed two times in PBS (WISSENT, Inc.), and left to recover for the indicated time. We determined that 20 μ M VP16 for 30 min was equivalent to \sim 2 Gy of IR by the neutral comet assay (Fig. S2 B). Alternately, asynchronous cell cultures were exposed to whole-cell IR (dose range, 0–20 Gy) using a 137 Cs irradiator (MDS Nordion) at 1 Gy/min (on ice, aerobic conditions). For kinase inhibition studies, cells were incubated with growth medium supplemented with 20 μ M wortmannin (Sigma-Aldrich), 5 mM caffeine (Sigma-Aldrich), 50 μ M LY294002, or 10 μ M Chk2 inhibitor II (EMD Biosciences, Inc.; Arienti et al., 2005) for 30 min, before addition of VP16 or exposure to IR. Cells were maintained in growth medium containing kinase inhibitors for the indicated time. For the inhibition of protein synthesis, cells were treated with 150 μ g/ml of cycloheximide (Sigma-Aldrich) for 30 min before treatments and maintained in cycloheximide until processed for LM.

IF detection of proteins, live-cell imaging, and FRAP

Cells grown on coverslips were treated with or without kinase or protein synthesis inhibitors before DSB induction (etoposide or IR), fixed, and processed for IF as previously described (Dellaire et al., 2006). Primary antibodies used in this study are as follows: rabbit anti-PML (CHEMICON International, Inc.); rabbit anti-Sp100 (CHEMICON International, Inc.); mouse anti-RPA (RPA34-20; Calbiochem); mouse anti-phospho-Histone H3 (ser10; clone MC463; Millipore); rabbit anti-cyclin A (sc-751; Santa Cruz Biotechnology, Inc.); mouse anti-SUMO-1 (GMP-1; Invitrogen); mouse anti- γ -H2AX (JBW301; Millipore). Secondary antibodies conjugated to Cy3 and Cy5 were obtained from Jackson ImmunoResearch Laboratories, and secondary antibodies conjugated to Alexa Fluor 488 were obtained from Invitrogen. DNA was stained with DAPI (Sigma-Aldrich) in mounting media containing 90% glycerol and 1 mg/ml paraphenylenediamine (Sigma-Aldrich). Fluorescence micrographs of fixed cells were collected using a 63 \times , 1.32 NA, oil-immersion objective lens (HCX PL APO CS; Leica) on an upright fluorescence microscope (DMR2; Leica) fitted with a camera (Orca; Hamamatsu). OpenLab 3.5.1 software (Improvision) was used for image acquisition. Live-cell imaging and FRAP analysis of GFP-PML IV in U-2 OS cells was performed as previously described (Dellaire et al., 2006). ImageJ v1.33 (National Institutes of Health) and Photoshop 7.0 (Adobe) software were used for image processing and analysis.

Statistical analysis

To determine mean PML NB number, maximum intensity projections of multiple focal planes were generated for the IF localization of PML using OpenLab 3.5.1 software (Improvision). PML NBs were counted in a minimum of 30 cells per time point and the NB number per cell was normalized for nucleus size. Normalization of NB number was accomplished by multiplying the ratio of the area of each nucleus divided by the mean area of a nucleus in a given dataset. This calculation was necessary to account for the variability in PML NB number caused by cell cycle phase or ploidy (Dellaire et al., 2006). However, in normal diploid cell lines, this calculation will not affect the mean NB number per cell, but will reduce statistical variability between datasets. Each experiment was repeated in triplicate, and the mean PML NB number was used directly or divided by the mean number of bodies in the control (untreated) to give the fold induction of PML NBs. Error analysis for triplicate experiments is expressed as the SEM, where SEM = SD \div $\sqrt{3}$. For all other experiments, error analysis was expressed simply as standard error. Datasets of PML NB number per cell exhibit a normal distribution; therefore, statistical significance between

datasets was derived using the *t* test for pair-wise analysis using Excel software (Microsoft) and by ANOVA for testing the significance of IR dose on PML NB number using online statistical tools available from <http://www.physics.csbsju.edu/stats/anova.html>. Curve fitting for PML NB induction versus dose of IR was accomplished online using tools available from <http://zunzun.com>.

Induction of subnuclear DNA damage by UV laser treatment

Cells grown on coverslips were incubated for 5 min in growth medium containing 0.5 μ g/ml of Hoechst 333258 to sensitize cells to the UV laser-induced damage. A confocal microscope (LSM 510; Carl Zeiss Microimaging, Inc.), equipped with an argon laser (488 nm) and tunable multiphoton laser (Chameleon; Coherent Inc.) capable of effective wavelengths in the UV range, was used to image cells and to generate UV laser-induced damage using a 63 \times , 1.40 NA, oil-immersion objective lens (Plan-Apochromat; Carl Zeiss Microimaging, Inc.). Laser damage was accomplished by selecting a region of interest (ROI) within a cell and bleaching the ROI using the tunable laser set at 790 nm (effective λ = 390 nm) and 20% power for a 200-ms pulse. At 2.40 NA, the laser generates 7–8 mW, which translates to a cellular dose of \sim 80 Gy (Bradshaw et al., 2005). Images were collected immediately after the bleach, using the argon laser at 50% power and 10% transmittance. Cells were maintained at 37°C during live-cell imaging, using a heated stage (Biopetechs).

Correlative LM/ESI

Samples were prepared and sectioned for correlative microscopy and ESI as previously described (Eskiw et al., 2003; Dellaire et al., 2004). Nitrogen and phosphorus maps were collected using a transmission electron microscope (Tecnaï 20; FEI) fitted with an electron imaging spectrometer (Gatan). Immunogold labeling was accomplished using a secondary antibody conjugated to Ultrasmall nanogold (donkey anti-rabbit; Electron Microscopy Sciences).

Online supplemental material

Fig. S1 shows the relative localization of PML NBs in respect to foci containing γ -H2AX, Nbs1, and RPA over time, after etoposide induced DSBs. Fig. S2 shows the mathematical modeling of PML NB number in response to IR-induced DSBs and compares the number of DSBs induced by 20 μ M etoposide versus varying doses of IR by neutral comet assay. Fig. S3 shows the biochemical composition of PML NBs over time after etoposide induced DSBs, in respect to SP100 and SUMO-1 content. Fig. S4 shows the effects of etoposide and caffeine, alone or in combination, on both the cell cycle profile and PML NB number of NHDFs. Table S1 shows the ANOVA analysis of PML NB number as a function of the dose of IR in NHDFs. Video 1 shows the fission of a PML microbody from a preexisting PML NB in response to DSBs induced by etoposide. Video 2 shows the loss of positional stability of PML NBs after UV laser induction of DSBs. Video 3 shows a control cell where, in the absence of UV laser-induced DSBs, PML NBs are positionally stable. Online supplemental material is available at <http://www.jcb.org/cgi/content/full/jcb.200604009/DC1>.

We thank Drs. J. Lukas, T. Mak, P. Nghiem, Y. Shiloh, J. Taylor, and B. Vogelstein for cell lines and plasmid reagents, Dr. Chet Tailor for his aid in retroviral transfections, and Ren Li for aid in preparing serial sections for the LM/ESIG. Dellaire is a Senior Postdoctoral Fellow of the Canadian Institutes of Health Research (CIHR), R.W. Ching is a recipient of a Restrcomp Studentship from The Hospital for Sick Children Research Institute, D.P. Bazett-Jones is a recipient of a Canada Research Chair in Molecular and Cellular Imaging, and R.G. Bristow is a Canadian Cancer Society Research Scientist.

This research was supported by operating grants from the CIHR to D.P. Bazett-Jones and the National Cancer Institute of Canada (grant 14246) to R.G. Bristow.

Submitted: 4 April 2006

Accepted: 1 September 2006

References

- Arienti, K.L., A. Brunmark, F.U. Axe, K. McClure, A. Lee, J. Blevitt, D.K. Neff, L. Huang, S. Crawford, C.R. Pandit, et al. 2005. Checkpoint kinase inhibitors: SAR and radioprotective properties of a series of 2-arylbenzimidazoles. *J. Med. Chem.* 48:1873–1885.
- Bernardi, R., P.P. Scaglioni, S. Bergmann, H.F. Horn, K.H. Vousden, and P.P. Pandolfi. 2004. PML regulates p53 stability by sequestering Mdm2 to the nucleolus. *Nat. Cell Biol.* 6:665–672.

- Bradshaw, P.S., D.J. Stavropoulos, and M.S. Meyn. 2005. Human telomeric protein TRF2 associates with genomic double-strand breaks as an early response to DNA damage. *Nat. Genet.* 37:193–197.
- Bristow, R.G., and R.P. Hill. 2005. Molecular and cellular basis of radiotherapy. In *The Basic Science of Oncology*, 4th edition. I.F. Tannock, R.P. Hill, R.G. Bristow, and L. Harrington, editors. McGraw-Hill, New York. 261–288.
- Buscemi, G., C. Savio, L. Zannini, F. Micciche, D. Masnada, M. Nakanishi, H. Tauchi, K. Komatsu, S. Mizutani, K. Khanna, et al. 2001. Chk2 activation dependence on Nbs1 after DNA damage. *Mol. Cell Biol.* 21:5214–5222.
- Carbone, R., M. Pearson, S. Minucci, and P.G. Pelicci. 2002. PML NBs associate with the hMre11 complex and p53 at sites of irradiation induced DNA damage. *Oncogene.* 21:1633–1640.
- Carney, J.P., R.S. Maser, H. Olivares, E.M. Davis, M. Le Beau, J.R. Yates III, L. Hays, W.F. Morgan, and J.H. Petrini. 1998. The hMre11/hRad50 protein complex and Nijmegen breakage syndrome: linkage of double-strand break repair to the cellular DNA damage response. *Cell.* 93:477–486.
- Chubb, J.R., S. Boyle, P. Perry, and W.A. Bickmore. 2002. Chromatin motion is constrained by association with nuclear compartments in human cells. *Curr. Biol.* 12:439–445.
- D'Amours, D., and S.P. Jackson. 2002. The Mre11 complex: at the crossroads of DNA repair and checkpoint signalling. *Nat. Rev. Mol. Cell Biol.* 3:317–327.
- Dellaire, G., and D.P. Bazett-Jones. 2004. PML nuclear bodies: dynamic sensors of DNA damage and cellular stress. *Bioessays.* 26:963–977.
- Dellaire, G., R. Farrall, and W.A. Bickmore. 2003. The Nuclear Protein Database (NPD): subnuclear localisation and functional annotation of the nuclear proteome. *Nucleic Acids Res.* 31:328–330.
- Dellaire, G., R. Nisman, and D.P. Bazett-Jones. 2004. Correlative light and electron spectroscopic imaging of chromatin in situ. *Methods Enzymol.* 375:456–478.
- Dellaire, G., R.W. Ching, H. Dehghani, Y. Ren, and D.P. Bazett-Jones. 2006. The number of PML nuclear bodies increases in early S phase by a fission mechanism. *J. Cell Sci.* 119:1026–1033.
- de Stanchina, E., E. Querido, M. Narita, R.V. Davuluri, P.P. Pandolfi, G. Ferbeyre, and S.W. Lowe. 2004. PML is a direct p53 target that modulates p53 effector functions. *Mol. Cell.* 13:523–535.
- D'Orazi, G., B. Cecchinelli, T. Bruno, I. Manni, Y. Higashimoto, S. Saito, M. Gostissa, S. Coen, A. Marchetti, G. Del Sal, et al. 2002. Homeodomain-interacting protein kinase-2 phosphorylates p53 at Ser 46 and mediates apoptosis. *Nat. Cell Biol.* 4:11–19.
- Esikiw, C.H., G. Dellaire, J.S. Mymryk, and D.P. Bazett-Jones. 2003. Size, position and dynamic behavior of PML nuclear bodies following cell stress as a paradigm for supramolecular trafficking and assembly. *J. Cell Sci.* 116:4455–4466.
- Esikiw, C.H., G. Dellaire, and D.P. Bazett-Jones. 2004. Chromatin contributes to structural integrity of promyelocytic leukemia bodies through a SUMO-1-independent mechanism. *J. Biol. Chem.* 279:9577–9585.
- Everett, R.D. 2001. DNA viruses and viral proteins that interact with PML nuclear bodies. *Oncogene.* 20:7266–7273.
- Everett, R.D., and J. Murray. 2005. ND10 components relocate to sites associated with herpes simplex virus type 1 nucleoprotein complexes during virus infection. *J. Virol.* 79:5078–5089.
- Gill, G. 2004. SUMO and ubiquitin in the nucleus: different functions, similar mechanisms? *Genes Dev.* 18:2046–2059.
- Gorisch, S.M., M. Wachsmuth, C. Itrich, C.P. Bacher, K. Rippe, and P. Lichter. 2004. Nuclear body movement is determined by chromatin accessibility and dynamics. *Proc. Natl. Acad. Sci. USA.* 101:13221–13226.
- Grobely, J.V., A.K. Godwin, and D. Broccoli. 2000. ALT-associated PML bodies are present in viable cells and are enriched in cells in the G(2)/M phase of the cell cycle. *J. Cell Sci.* 113:4577–4585.
- Guo, A., P. Salomoni, J. Luo, A. Shih, S. Zhong, W. Gu, and P.P. Pandolfi. 2000. The function of PML in p53-dependent apoptosis. *Nat. Cell Biol.* 2:730–736.
- Hofmann, T.G., A. Moller, H. Sirma, H. Zentgraf, Y. Taya, W. Droge, H. Will, and M.L. Schmitz. 2002. Regulation of p53 activity by its interaction with homeodomain-interacting protein kinase-2. *Nat. Cell Biol.* 4:1–10.
- Hu, P., S.F. Beresten, A.J. van Brabant, T.Z. Ye, P.P. Pandolfi, F.B. Johnson, L. Guarente, and N.A. Ellis. 2001. Evidence for BLM and Topoisomerase IIIalpha interaction in genomic stability. *Hum. Mol. Genet.* 10:1287–1298.
- Koi, M., A. Umar, D.P. Chauhan, S.P. Cherian, J.M. Carethers, A. Kunkel, and C.R. Boland. 1994. Human chromosome 3 corrects mismatch repair deficiency and microsatellite instability and reduces N-methyl-N'-nitro-N-nitrosoguanidine tolerance in colon tumor cells with homozygous hMLH1 mutation. *Cancer Res.* 54:4308–4312.
- Kruhlak, M.J., A. Celeste, G. Dellaire, O. Fernandez-Capetillo, W.G. Muller, J.G. McNally, D.P. Bazett-Jones, and A. Nussenzweig. 2006. Changes in chromatin structure and mobility in living cells at sites of DNA double-strand breaks. *J. Cell Biol.* 172:823–834.
- Kurz, E.U., and S.P. Lees-Miller. 2004. DNA damage-induced activation of ATM and ATM-dependent signaling pathways. *DNA Repair (Amst.).* 3:889–900.
- Lydall, D., and S. Whitehall. 2005. Chromatin and the DNA damage response. *DNA Repair (Amst.).* 4:1195–1207.
- Nghiem, P., P.K. Park, Y. Kim, C. Vaziri, and S.L. Schreiber. 2001. ATR inhibition selectively sensitizes G1 checkpoint-deficient cells to lethal premature chromatin condensation. *Proc. Natl. Acad. Sci. USA.* 98:9092–9097.
- O'Driscoll, M., V.L. Ruiz-Perez, C.G. Woods, P.A. Jeggo, and J.A. Goodship. 2003. A splicing mutation affecting expression of ataxia-telangiectasia and Rad3-related protein (ATR) results in Seckel syndrome. *Nat. Genet.* 33:497–501.
- Pommier, Y., O. Sordet, V.A. Rao, H. Zhang, and K.W. Kohn. 2005. Targeting chk2 kinase: molecular interaction maps and therapeutic rationale. *Curr. Pharm. Des.* 11:2855–2872.
- Rao, V.A., A.M. Fan, L. Meng, C.F. Doe, P.S. North, I.D. Hickson, and Y. Pommier. 2005. Phosphorylation of BLM, dissociation from topoisomerase IIIalpha, and colocalization with gamma-H2AX after topoisomerase I-induced replication damage. *Mol. Cell Biol.* 25:8925–8937.
- Rogakou, E.P., C. Boon, C. Redon, and W.M. Bonner. 1999. Megabase chromatin domains involved in DNA double-strand breaks in vivo. *J. Cell Biol.* 146:905–916.
- Salomoni, P., and P.P. Pandolfi. 2002. The role of PML in tumor suppression. *Cell.* 108:165–170.
- Seker, H., C. Rubbi, S.P. Linke, E.D. Bowman, S. Garfield, L. Hansen, K.L. Borden, J. Milner, and C.C. Harris. 2003. UV-C-induced DNA damage leads to p53-dependent nuclear trafficking of PML. *Oncogene.* 22:1620–1628.
- Shiloh, Y. 2001. ATM and ATR: networking cellular responses to DNA damage. *Curr. Opin. Genet. Dev.* 11:71–77.
- Stewart, G.S., R.S. Maser, T. Stankovic, D.A. Bressan, M.I. Kaplan, N.G. Jaspers, A. Raams, P.J. Byrd, J.H. Petrini, and A.M. Taylor. 1999. The DNA double-strand break repair gene hMRE11 is mutated in individuals with an ataxia-telangiectasia-like disorder. *Cell.* 99:577–587.
- Xu, Z.X., A. Timanova-Atanasova, R.X. Zhao, and K.S. Chang. 2003. PML colocalizes with and stabilizes the DNA damage response protein TopBP1. *Mol. Cell Biol.* 23:4247–4256.
- Yang, S., C. Kuo, J.E. Bisi, and M.K. Kim. 2002. PML-dependent apoptosis after DNA damage is regulated by the checkpoint kinase hCds1/Chk2. *Nat. Cell Biol.* 4:865–870.
- Yeager, T.R., A.A. Neumann, A. Englezou, L.I. Huschtscha, J.R. Noble, and R.R. Reddel. 1999. Telomerase-negative immortalized human cells contain a novel type of promyelocytic leukemia (PML) body. *Cancer Res.* 59:4175–4179.
- Zhong, S., P. Salomoni, and P.P. Pandolfi. 2000. The transcriptional role of PML and the nuclear body. *Nat. Cell Biol.* 2:E85–E90.